Journal of Cerebral Blood Flow & Metabolism (2012) 32, 318–329

www.jcbfm.com

Neocortical capillary flow pulsatility is not elevated in experimental communicating hydrocephalus

Shams Rashid[1], James P McAllister II[2], Yiting Yu[3] and Mark E Wagshul[4,5]

[1]*Department of Biomedical Engineering, Stony Brook University, Stony Brook, New York, USA;* [2]*Division of Pediatric Neurosurgery, Department of Neurological Surgery, University of Utah, Salt Lake City, Utah, USA;* [3]*Department of Epidemiology and Population Health, Albert Einstein College of Medicine, Bronx, New York, USA;* [4]*Departments of Radiology and Biophysics, Gruss MRRC, Albert Einstein College of Medicine, Bronx, New York, USA;* [5]*Department of Radiology, Stony Brook University, Stony Brook, New York, USA*

While communicating hydrocephalus (CH) is often characterized by increased pulsatile flow of cerebrospinal fluid (CSF) in the cerebral aqueduct, a clear-cut explanation for this phenomenon is lacking. Increased pulsatility of the entire cerebral vasculature including the cortical capillaries has been suggested as a causative mechanism. To test this theory, we used two-photon microscopy to measure flow pulsatility in neocortical capillaries 40 to 500 μm below the pial surface in adult rats with CH at 5 to 7 days (acute, $n=8$) and 3 to 5 weeks (chronic, $n=5$) after induction compared with intact controls ($n=9$). Averaging over all cortical depths, no increase in capillary pulsatility occurred in acute (pulsatility index (PI): 0.15 ± 0.06) or chronic (0.14 ± 0.05) CH animals compared with controls (0.18 ± 0.07; $P=0.07$). More specifically, PI increased significantly with cortical depth in controls ($r=0.35$, $P<0.001$), but no such increase occurred in acute ($r=0.06$, $P=0.3$) or chronic ($r=0.05$, $P=0.5$) CH. Pulsatile CSF aqueductal flow, in contrast, was elevated 10- to 500-fold compared with controls. We conclude that even in the presence of markedly elevated pulsatile CSF flow in the aqueduct, there is no concurrent increase in microvascular pulsatile flow.
Journal of Cerebral Blood Flow & Metabolism (2012) **32,** 318–329; doi:10.1038/jcbfm.2011.130; published online 21 September 2011

Keywords: animal studies; brain imaging; capillaries; cerebral blood flow measurement; two-photon microscopy

Introduction

While it is well known that cerebrospinal fluid (CSF) flow in the cranium has a marked cardiac-induced pulsatile component, whether CSF pulsatility has an important role in disease remains a topic of ongoing debate. A number of studies have linked alterations in pulsatile CSF flow with various pathologies, such as hydrocephalus (Bradley *et al*, 1996; Luetmer *et al*, 2002; Wagshul *et al*, 2009), syringomyelia (Mauer *et al*, 2008), and Chiari malformations (Alperin *et al*, 2005; Quigley *et al*, 2004), but these associations do not give any indication for a causative role of CSF pulsatility in these conditions. On a more fundamental level, while elevated CSF flow pulsations in the cerebral aqueduct have been shown in numerous studies, mostly in normal pressure hydrocephalus (Bateman and Loiselle, 2007; Bradley *et al*, 1996; Kahlon *et al*, 2007; Luetmer *et al*, 2002; Miyati *et al*, 2003), the exact mechanism for elevated pulsatility is still debated. Until the driving mechanism behind elevated CSF flow pulsatility is well understood, it is uncertain how this potential marker of disease and recovery in hydrocephalus can serve as an acceptable prognostic tool.

It has been suggested that the increase in CSF pulsatility in communicating hydrocephalus (CH) stems from changes in the compliance of the subarachnoid space, leading to a redistribution of the subarachnoid space CSF flow pulsatility into the brain microvasculature (Greitz, 1993). This would explain the increase in macroscopic pulsations in the cerebral aqueduct, because of the mechanical coupling between the ventricular walls and the parenchyma. However, a potentially more significant implication of this theory would be an overall increase in vascular pulsations throughout the brain, including the cerebral microvasculature. Increased microvascular pulsatility can have pathological implications, because increased pulsatile stress forces can activate potent vasoactive factors (Bilfinger and Stefano, 2000; Silacci *et al*, 2001; Ziegler *et al*, 1998). However, the primary counter theory suggests that increased CSF pulsations are simply a product of the reduced intracranial compliance, due to either increased intracranial pressure

Correspondence: Dr ME Wagshul, 1300 Morris Park Avenue, Gruss MRRC 208, Bronx, NY 10461, USA.
E-mail: mark.wagshul@einstein.yu.edu
Received 3 February 2011; revised 5 July 2011; accepted 22 August 2011; published online 21 September 2011

or tissue compression from the expanded ventricles, resulting in elevated brain pulsations as dictated by the exponential pressure–volume curve (Marmarou *et al*, 1975). This theory would imply that while pressure pulsations in the brain may be increased in hydrocephalus, these may not be accompanied by any change in microvascular flow pulsatility.

Thus, the primary purpose of this study was to test the theory that pulsations in microvascular flow are elevated in hydrocephalus, and that these are associated with elevated aqueductal flow pulsations. We used two-photon laser-scanning microscopy (Denk *et al*, 1990; Kleinfeld *et al*, 1998) to quantify microvascular flow pulsations *in vivo* and to probe their changes with the development of hydrocephalus. Using our recently developed rat model of CH (Li *et al*, 2008), with varying degrees of disease severity and marked elevation of CSF pulsation in the aqueduct (Wagshul *et al*, 2009), we studied capillary pulsatility at both the acute and chronic phases. The main objectives of the study were to determine the normal levels of capillary pulsatility in the rat neocortex, whether this pulsatility is elevated in CH, and to what extent pulsatility is related to aqueductal CSF pulsations and the degree of ventriculomegaly.

Materials and methods

All experimental procedures were performed in accordance with the NIH Guide for Care and Use of Laboratory Animals, and approved by the Institutional Animal Care and Use Committee of Stony Brook University (Stony Brook, NY). Every effort was taken to minimize the discomfort and the number of animals used.

Communicating Hydrocephalus Induction and Study Design

Twenty-five female Sprague-Dawley rats (200 to 250 g) were included in this study. Communicating hydrocephalus was induced in 16 rats by injecting kaolin into the basal cisterns, using the technique developed by us (Li *et al*, 2008); nine animals served as controls. Postoperatively, animals exhibiting lethargy and weight loss received subcutaneous supplements of 5% dextrose and Ringer's lactate for 3 to 5 days. Multiphoton microscopy was performed at either the acute (5 to 7 days after induction, $n = 8$) or the chronic (3 to 5 weeks after induction, $n = 8$) stage of hydrocephalus development. Hydrocephalus was characterized a few days before multiphoton microscopy by magnetic resonance imaging to quantify the volume of the cerebral ventricles and the stroke volume (SV) of pulsatile CSF flow at the cerebral aqueduct, as described previously (Wagshul *et al*, 2009). Animals with a ventricular volume (VV) $> 30\,\mu$L were considered hydrocephalic; this criterion had been established in a previous study (Wagshul *et al*, 2009). Kaolin animals that failed to develop hydrocephalus by this criterion were excluded from the study.

Two-Photon Microscopy

An optically transparent cranial window was opened in the right parietal bone to provide access to neocortical capillaries for imaging. Each animal was anesthetized with an intraperitoneal injection of ketamine/xylazine (70/7 mg/kg) and secured to a custom-made head holder with ear bars. The head was shaved, the skin incised and a 5×3 mm craniectomy, centered ~ 5 mm posterior and 2.5 mm lateral to Bregma, was made by thinning the bone along the periphery and then carefully removing the bone flap. The drilling area was irrigated frequently with cold saline to prevent heating of the underlying tissue; the dura was left intact in all animals. A styptic pad was gently applied to the dura to stop any bleeding. The craniectomy was then filled with warm 1% agarose and covered with a custom-cut glass coverslip, which was then sealed to the skull with cyanoacrylate gel. The sealed cranial window served to maintain normal intracranial pressure and flow dynamics. A metal plate with a 3×1 cm opening surrounding the craniectomy was attached to the skull with cyanoacrylate gel and screwed to the head holder to prevent further head motion.

Multiphoton imaging was performed on an Olympus BX60WI microscope (Olympus America Inc., Center Valley, PA, USA), equipped with a 1.7-W Chameleon laser (Coherent Inc., Santa Clara, CA, USA), and a $60\times$ water immersion objective. After the animal was positioned under the microscope, 0.5 mL of 70 kDa fluorescein isothiocyanate dextran (Sigma, St Louis, MO, USA), dissolved in 1 mol/L PBS at 40 mg/mL, was injected through the tail vein. The fluorophore labels blood serum but is not taken up by red blood cells (RBCs), causing them to appear as dark moving objects against the bright, labeled serum. Optimal two-photon excitation was at 800 nm.

Capillaries were imaged at 2 to 4 nonoverlapping sites within the cranial window with a total of 20 to 40 capillaries in each animal, at depths of 40 to 500 μm; all depths were measured from the pial surface. They exclude the thickness of the dura and cover cortical layers 1 to 3; the dorsal edge of layer 4 is $\sim 500\,\mu$m from the pial surface in control rats. Capillaries were visualized by 2D planar scans (Figure 1A), which were later used for vessel diameter determination. Capillaries selected for flow measurements had a straight in-plane length of at least 10 μm. Individual line scans were ~ 16 seconds long with temporal resolution of 1.6 ± 0.3 ms per line and spatial extent of $26 \pm 4\,\mu$m (Figure 1D). The microscope was controlled by FluoView FV300 software (Olympus Inc.) running on a desktop PC.

Anesthesia was maintained throughout imaging with 50% supplements of the initial ketamine/xylazine dose, as needed. Electrocardiogram pads were attached to the animal's fore and hind paws, and the electrocardiogram was recorded continuously for anesthesia monitoring and heart rate (HR) determination in the data processing. Animals were euthanized at the end of the imaging session by an overdose of pentobarbital.

Image Processing

All image processing and data analysis were performed using Matlab applications (The Mathworks, Natick, MA,

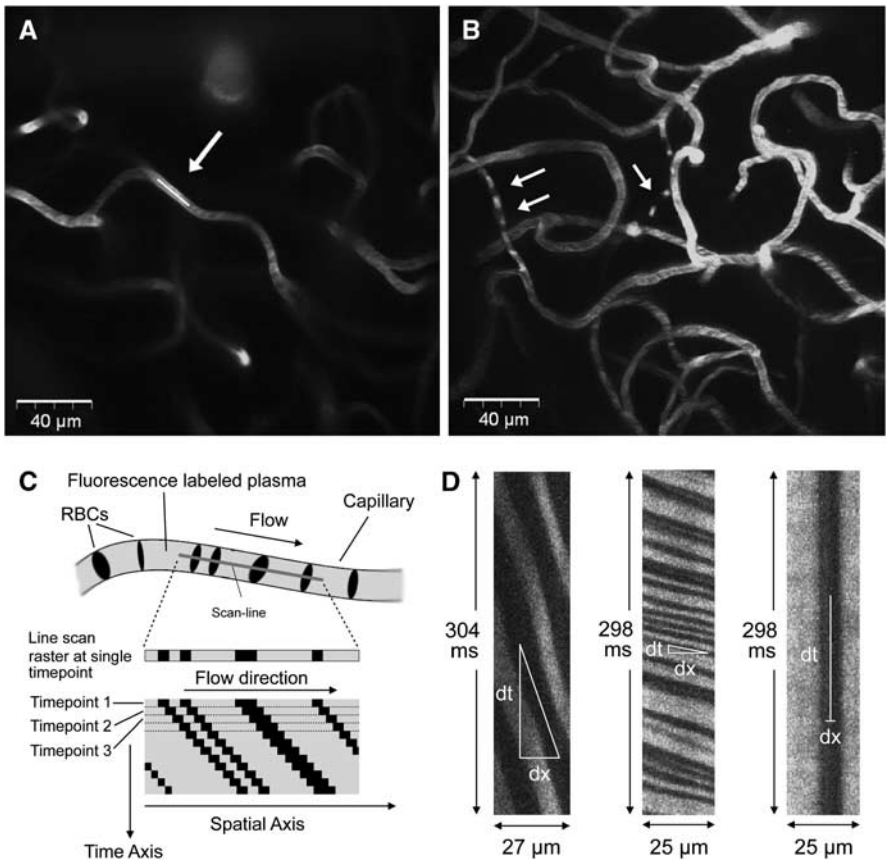

Figure 1 A 2D planar image showing a section of a capillary network, at a depth of 160 μm, in a control animal. The white line indicates the line over which the capillary was scanned (**A**). A maximum intensity projection in a chronic communicating hydrocephalus (CH) animal showing a microvascular network in the depth range of 185 to 250 μm. White arrows indicate vessels with flowing red blood cells (RBCs), which appear as dark voids against the bright labeled plasma (**B**). A line-scan image is formed from multiple, repeat acquisitions over time of the same line (the scan line) along the central axis of a vessel, as depicted in this cartoon (**C**). In a line scan, the horizontal axis represents the spatial length of the scan line, while time increases along the vertical axis. In any single scan line, each nonfluorescent-labeled RBC appears as a dark band against a bright backdrop of fluorescence-labeled serum. Each successive line is stacked beneath the previous acquired line in the image. As a result, moving RBCs form diagonal dark bands. The horizontal extent of each band represents the distance traversed by the RBC, while the vertical extent represents the time taken to traverse that distance. Thus, velocity of each RBC is given by the inverse of the slope of the RBC band (i.e., rapid-moving RBCs have shallow slopes and slow-moving RBCs have steep slopes). Sample, partial line-scan images are shown in (**D**), with RBCs having slow flow (left), rapid flow (middle), and no flow (right, i.e., its position in the capillary does not change with time). The colour reproduction of this figure is available on the *Journal of Cerebral Blood Flow and Metabolism* journal online.

USA). Moving RBCs form dark bands in the line-scan image (Figure 1C) so that RBC velocity at any given point on the image is related to the slope of the bands. To calculate the velocity as a function of time, the line-scan image was broken into small time segments of $\sim$45 ms, which were overlapped to produce an effective temporal resolution of $\sim$15 ms per data point. Slopes were calculated for each segment using the singular value decomposition method first described by Kleinfeld *et al* (1998), as follows: the segment was rotated incrementally through a range of angles, and a parameter p was calculated for each angle α, as given by equation (1):

$$p(\alpha) = \frac{(s_1(\alpha))^2}{\sum_{n=1}^{m} (s_n(\alpha))^2} \quad (1)$$

where s is a $m \times 1$ array of the singular values of the $m \times m$ image segment, rotated by angle α. Parameter p has a maximum when the bands in the rotated image segment become horizontal and thus determines the slope of the bands and, by extension, RBC velocity. The singular value decomposition calculation was repeated for each segment to produce a velocity waveform for the entire duration of the line-scan image. Segment size and spacing were chosen taking into consideration velocity accuracy, temporal resolution in the final velocity waveform, and computational speed. Preliminary calculations were also performed at a slightly lower temporal resolution ($\sim$30 ms), but there was a small but statistically significant drop in pulsatility index (PI) for all animals of 6% to 10% compared with the higher temporal resolution analyses. While the higher temporal resolution also led to more vessel measurements being excluded due to spike artifacts (at higher resolution, periods with no RBC's become more frequent), we felt this was the better choice to ensure accurate PI measurements.

Line-scan images of poor quality (e.g., RBC bands not visually distinguishable) and images with severe motion artifacts were excluded from analysis. Single-point spikes in the velocity waveform, usually due to either small motion artifacts or low RBC density, were corrected automatically with a median filter; data sets with <4 contiguous seconds of spike-free velocity data were discarded.

Pulsatility Index

Pulsatility was quantified from the velocity waveforms with the Gosling PI, the ratio of the mean peak-to-peak amplitude of the waveform to its mean velocity, typically calculated in the time domain (Gosling and King, 1974). However, to limit pulsatility calculations to cardiac-induced pulsations, PI was computed in the frequency domain from the power spectrum of the velocity waveform by integrating over the cardiac frequency peak and its second harmonic, which were identified using the animal's HR extracted from the electrocardiogram waveform. This integral was then divided by the first bin of the power spectrum, which equals the mean velocity, to produce the PI. A baseline, computed from the average of the spectral points immediately adjacent to the peaks, was subtracted before PI calculation to remove the effects of background noise.

Calculation of Vessel Diameter

Capillary diameters were measured from 2D planar scans by selecting a profile perpendicular to the axis of the capillary, averaged over the segment through which flow was measured. A flat-topped function with Gaussian edges was fitted to this profile, and diameter was measured as the full-width at half-maximum of the function.

Statistical Analyses

Differences in vessel diameter, vessel depth, and HR between the three experimental groups (acute CH, chronic CH, and controls) were compared using one-way repeated measures analysis of variance.

Pulsatility indices were compared among the three experimental groups using two linear mixed models, treating repeated measures in each animal as a random effect and controlling for vessel diameter, vessel depth, and HR, all of which varied randomly within the data sets. In one model, fixed effects of experimental group, diameter, depth, and HR on PI were tested. In a second model, three interaction terms group by depth, group by diameter, and group by HR were added to the model to test for differences within the groups based on linear variations in PI with these varying experimental parameters.

Based on the results of these initial models showing significant group by depth and group by HR interactions, *post hoc* analysis was performed to identify specific subgroups of depth and HR ranges contributing to differences between the groups. Pulsatility index data were split into six subgroups: three depth ranges (<200, 200 to 300, and $>300\,\mu$m) and each with two HR ranges (low and high HR, separated by the median HR of 240 beats per minute). Within each subgroup, PI was then compared between experimental groups using repeated measures analysis of variance.

Pearson correlations were used to examine the association between capillary PI (calculated for each animal, averaged over all vessels) and aqueductal SV. Similarly, Pearson correlations between PI and VV were also used to determine the relationship between capillary pulsatility and ventricular dilation.

All data are reported as mean ± standard deviation. Normal distribution of data was verified using histograms. Statistical computations were performed in SAS (SAS Institute Inc., Cary, NC, USA), and results were considered significant at $P<0.05$.

Results

Communicating Hydrocephalus Induction

Three chronic animals did not develop hydrocephalus and were excluded from analysis. Figure 2 illustrates the marked difference in ventricular size between hydrocephalic and control animals. Mean VV was 132 ± 31 and $77\pm31\,\mu$L for the acute and chronic groups, respectively; the difference between these groups was significant ($P<0.01$). Mean CSF SV was 256 ± 96 and $30\pm19\,$nL for the acute and chronic animals, respectively; this difference was also significant ($P<0.01$). While magnetic resonance imaging was not performed on intact control animals, previous studies have shown that these values for both VV and SV are significantly elevated compared with normal control values (VV: $15.5\pm2.0\,\mu$L, SV: $0.72\pm0.13\,$nL; Wagshul *et al*, 2009).

Two-Photon Microscopy

Nineteen percent of line-scan images were discarded due to the presence of artifacts, poor quality, or abnormal flow. In some images, cardiac- or respiratory-induced pulsations caused excessive vessel motion and periodic motion artifacts in the line-scan images. Images with very low RBC density resulted in large data segments with no RBCs, and thus no recognizable features for the velocity calculation. This was the primary cause of spikes in the extracted velocity waveform, and as noted above, data sets with <4 seconds of continuous RBC motion were excluded. In some vessels, blood flow in a capillary slowed or stopped, and then resumed after a few seconds or even minutes. In rare cases, flow would reverse direction. In images with such artifacts or aberrant flow, the portion of the image containing the artifact(s) or arrested flow was discarded, and only the portion of the image with good contrast was used for velocity waveform analysis.

Valid RBC velocity waveforms were collected in 765 capillaries (323 acute CH, 184 chronic CH, and 258 intact controls). Average depth of capillaries for all animals was $254\pm90\,\mu$m beneath the pial surface; all capillaries were deeper than $40\,\mu$m, with one third

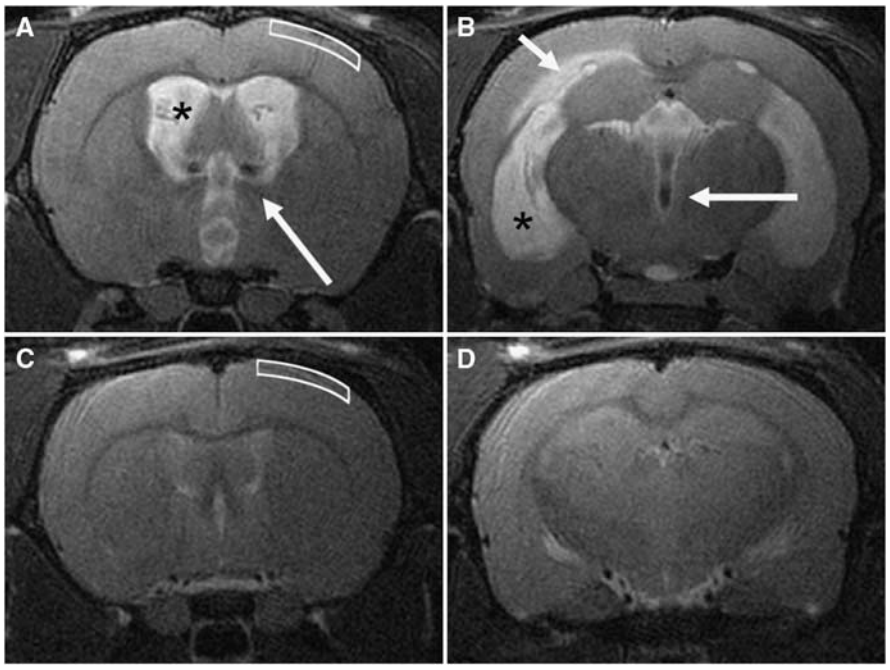

Figure 2 Representative T2-weighted coronal magnetic resonance images at the level of the foramen of Monro (**A**, **C**) and the temporal horn of the lateral ventricles (**B**, **D**). In the acute communicating hydrocephalus (CH) rat (**A**, **B**), the lateral ventricles (asterisks) and third ventricle were markedly dilated. In some animals, the periventricular white matter was edematous (short arrow), and flow voids due to elevated cerebrospinal fluid (CSF) pulsatility were usually noticeable (long arrows). This pattern was also observed in chronic CH animals (not shown). In a control rat (**C**, **D**) the lateral ventricles were slitlike and no edema was found in the periventricular white matter. The white boxes (**A**, **C**) show the region of the cortex imaged by microscopy, to a depth of $\sim 500\,\mu$m from the pial surface, primarily covering cortical layers 2 and 3 (the dorsal edge of layer 4 lies at $\sim 500\,\mu$m in a control animal).

deeper than $300\,\mu$m, and the deepest capillary was imaged at $549\,\mu$m. The maximum depth achieved in each animal depended mainly on the quality of the cranial window. Because the dura was left intact, capillaries could not be visualized in most animals beneath $450\,\mu$m. Mean capillary depths for the acute, chronic, and control groups were 276 ± 78, 259 ± 98, and $242 \pm 99\,\mu$m, respectively; the depth for the control group was significantly smaller than that of the acute group ($P < 0.02$). Mean capillary diameters were 4.4 ± 0.7, 4.5 ± 0.8, and $4.7 \pm 1.0\,\mu$m for the acute, chronic, and control animals, respectively. Diameters for the control animals were significantly larger than that of both acute and chronic animals ($P < 0.001$ and $P < 0.05$, respectively). Mean HRs were 276 ± 72, 224 ± 45, and 240 ± 58 beats per minute for the acute, chronic, and control animals, respectively; these differences were not statistically significant. While mean blood flow was not the focus of our work, flow rates extracted from our mean flow velocities and capillary diameter data were 0.6 ± 0.6, 0.8 ± 0.7, and 0.8 ± 0.9 nL/min for the acute, chronic, and control animals, respectively; blood flow in the acute group was significantly lower than in the control group ($P < 0.001$).

Capillary Pulsatility

Most waveforms were clearly pulsatile, with a distinct frequency peak at the electrocardiogram-derived HR. Two representative examples of line-scan images, and their associated velocity waveforms and frequency spectra, are shown in Figure 3.

The highly significant, linear relationship between absolute pulse amplitude and mean flow velocity for all measurements in the study, illustrated in Figure 4, provides good justification of the choice of PI, the ratio of pulse amplitude to mean velocity, as a measure of flow pulsatility which is minimally influenced by variations in vessel caliber and mean flow velocity. Pulsatility indices for the acute, chronic, and control groups, as analyzed in the first linear mixed model without controlling for HR, depth or vessel size, are shown in Figure 5. Pulsatility indices were 0.15 ± 0.06 (acute), 0.14 ± 0.05 (chronic), and 0.18 ± 0.07 (control); although there was a trend toward lower PIs for the hydrocephalic animals, this was not statistically significant ($P = 0.07$). However, PI varied significantly over vessel depth ($P < 0.0005$), HR ($P < 0.0001$), and diameter ($P = 0.02$).

The second linear mixed model, which did control for these experimental parameters, showed that PI was significantly larger in controls compared with both acute and chronic animals ($P < 0.0001$ and $P < 0.005$), when accounting for varying depth, diameter, and HR. The association between PI and depth differed significantly across the groups: in controls, PI increased with increasing depth (0.02 for every $100\,\mu$m), while there was no increase in PI with depth for either CH groups (control versus acute:

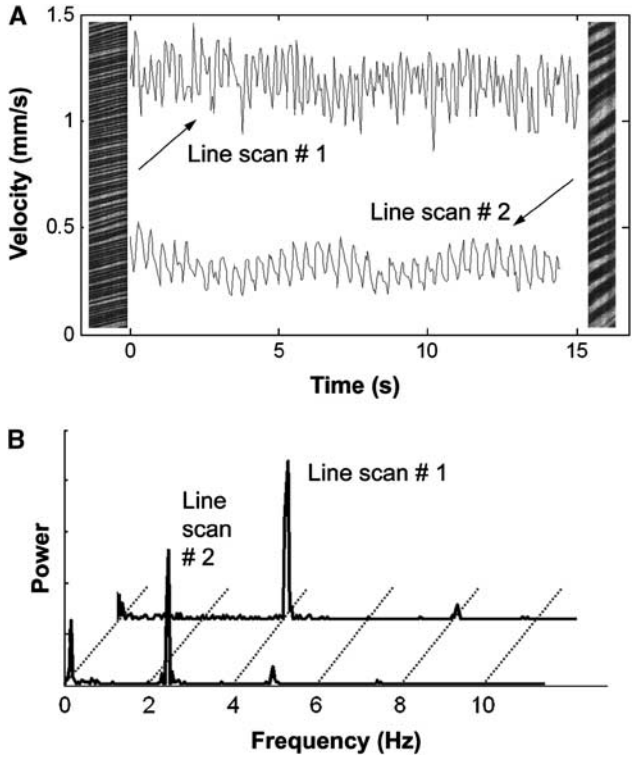

Figure 3 Two representative line scans with their corresponding velocity waveforms (**A**). The line scan on the left (line scan #1) has rapid flow (mean velocity = 1.18 mm/s), while the one on the right (line scan # 2) has slower flow (mean velocity = 0.32 mm/s). Pulsatility can be clearly seen in the waveforms; pulsatility indices (PIs) were 0.41 and 0.14, respectively. As discussed in Materials and methods section, PI for each line scan was calculated in the frequency domain by integrating over these peaks to extract a cardiac-induced pulsatility measure only. Indeed, the corresponding power spectra (**B**) verify that the pulsatility is primarily cardiac in nature, as is evident from the prominent frequency components at the heart rate frequencies (4.0 and 2.5 Hz for these two vessels, respectively).

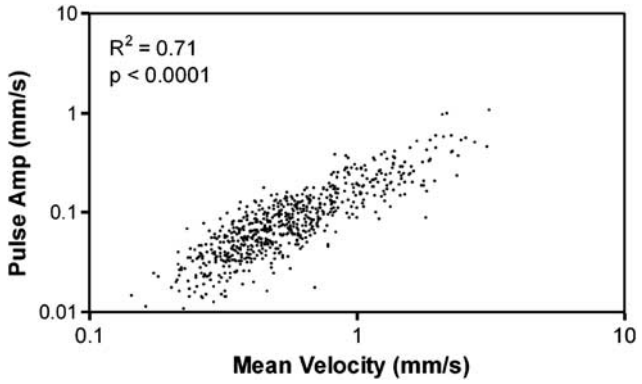

Figure 4 Linear relationship between absolute pulse amplitude and mean velocity plotted for all vessels and all experimental groups in the study. The highly significant, linear relationship provides the justification for using the ratio between pulse amplitude and mean velocity, the pulsatility index (PI), as the experimental measure of choice. The use of PI minimizes the variability of pulsatility measurements due to changes in absolute blood flow, which is well known to be lowered in hydrocephalus and was in fact found to be lower in the acute group.

$P<0.05$ and control versus chronic: $P<0.0005$; Figure 6, left). The association between PI and HR also differed significantly across the groups ($P<0.0001$). Pulsatility index increased in the control group with HR (0.08 for every 100 beats per minute), but not in the acute and chronic CH groups (control versus acute: $P<0.0001$ and control versus chronic: $P<0.005$). The association between PI and vessel diameter did not differ significantly across the groups ($P=0.24$). In summary, PI increased significantly with depth and HR in the controls, but not in the acute or chronic animals.

Post hoc analysis showed that PI differences between control and hydrocephalic animals were most prominent in the high HR-largest depth subgroup (Figure 6, lower right). Although this difference was not statistically significant because of the small number of vessels in this subgroup, there was a trend toward higher PI in the control group ($P=0.08$). In addition, PI was significantly increased in controls compared with chronic CH animals, in the low HR-largest depth subgroup ($P=0.03$) (Figure 6, upper right). Thus, while the subgrouping weakened the statistical significance, the *post hoc* analyses in general showed that the PI differences between the control and hydrocephalic groups were primarily driven by increased PI in the control group in the largest depth vessels.

Pulsatility index results for the acute and chronic CH animals, averaged over all vessels in each animal, were compared with their CSF SVs and VVs (Figure 7). No correlation was found between either VV or aqueductal CSF SV and PI, for either acute or chronic CH animals. Based on prior measurements of CSF SV in intact control animals (Wagshul *et al*, 2009), we can conclude that there is no increase in microvascular flow pulsatility, even in the presence of a 10- to 500-fold increase in ventricular CSF pulsatility as measured at the cerebral aqueduct.

Discussion

We have shown the feasibility of measuring flow pulsatility in the live rat neocortex from the pial surface to depths of 500 μm. We have applied the technique to measurements in a rat model of CH, although the technique is easily translatable to other small animal models and opens up the possibility of microvascular pulsatility studies in a broader context, such as stroke and atherosclerosis. Contrary to our initial hypothesis, our results indicate that pulsatility of capillary blood flow in the rat neocortex is not elevated in hydrocephalus. Statistical analyses accounting for multiple experimental factors also demonstrated a new finding: a significant increase in capillary pulsatility with depth from the pial surface in control animals that disappears in hydrocephalus.

Relationship of Pulsatility with Vessel Depth, Diameter, and Heart Rate

Three parameters were examined to assess their effect on pulsatility: depth of the vessels from the pial surface, vessel diameter, and HR. In control animals, our results show a complex dependence of pulsatility on all three parameters. Vessel diameter is expected to affect mean flow velocity, and therefore, absolute pulse amplitude. Studies documenting changes in capillary morphology also show that cortical capillary density is altered in hydrocephalus (Jones *et al*, 1991; Luciano *et al*, 2001). Such effects may give rise to changes in mean blood flow and absolute pulse amplitude in capillaries, but should not affect their ratio. Thus, to mitigate the effect of vessel diameter and density on our results, PI was chosen as the outcome measure. Our results do show a very small increase in pulsatility with vessel diameter, which may be related to changes in effective vessel compliance with size. However, there was no difference in this dependence between experimental groups, indicating that any differences in compliance between the groups that might lead to changes in pulsatility are driven by factors unrelated to vessel morphology but more likely driven by extravascular factors.

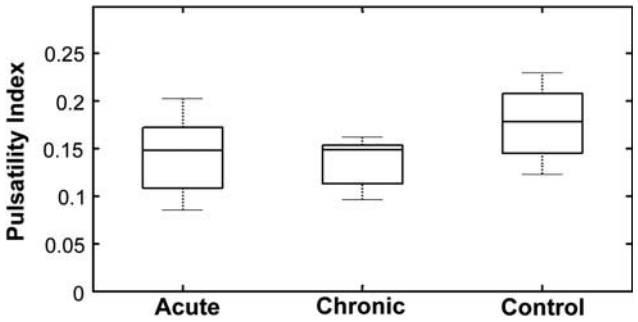

Figure 5 Boxplots of pulsatility index for the acute, chronic, and control groups. Without accounting for variations in vessel diameter, depth, or heart rate, there was no significant difference between the groups, other than a trend toward higher pulsatility in controls ($P = 0.07$).

In contrast, PI showed a much stronger dependence on depth, increasing significantly with depth, in controls only. Similarly, the positive relationship between pulsatility and HR in control animals was not present in the hydrocephalic animals. Based

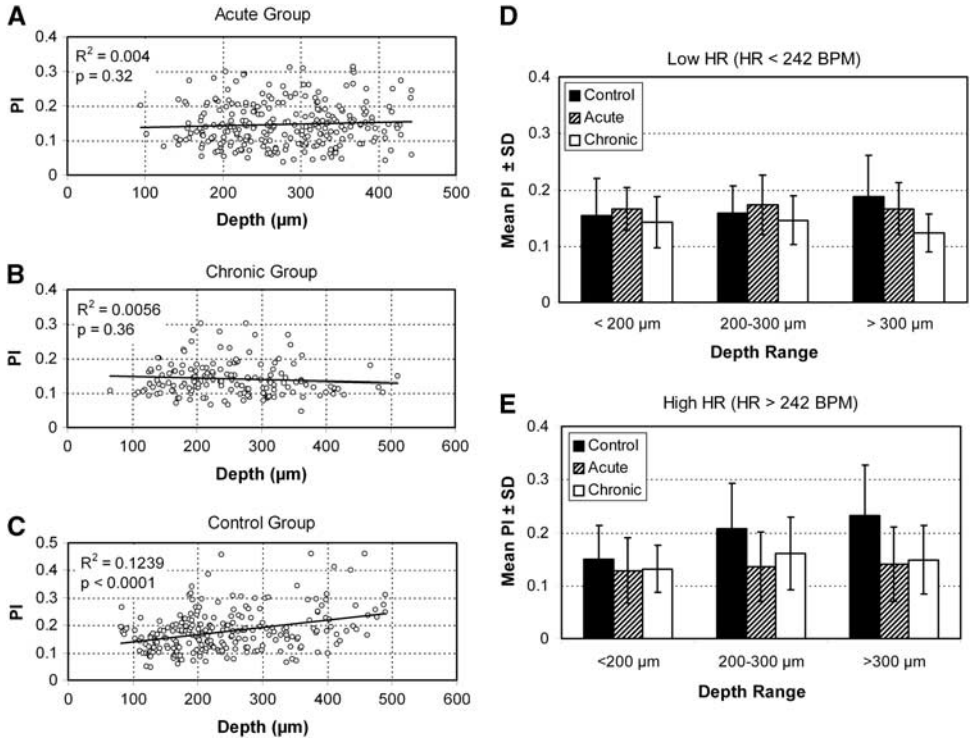

Figure 6 The effect of vessel depth on pulsatility index (PI) in the three experimental groups (**A**–**C**). Linear mixed model analyses revealed a significant depth association in the controls, with pulsatility increasing with increasing depth from the pial surface, but no such relationship in either of the hydrocephalic groups. There was also a significant association between PI and HR in the control group, again with PI increasing with the higher HRs (not shown). *Post hoc* analyses using subgrouping of the data according to depth and HR were used to confirm that the differences between the groups were primarily being driven by increased pulsatility in the deeper vessels of control animals compared with the hydrocephalic animals in similar depth vessels (**D**, **E**). The statistical significance of these tests was dramatically impacted due to the smaller number of vessels in each individual subgroup. Nonetheless, the increase in pulsatility for control animals with depth can be clearly seen in both graphs, and the increase in pulsatility for deeper vessel in controls compared with hydrocephalics is now starkly evident.

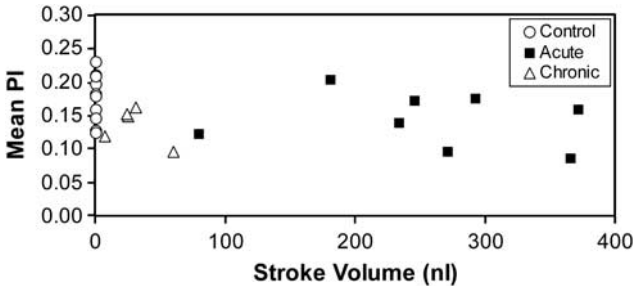

Figure 7 Mean pulsatility index (PI), averaged by animals, for both acute and chronic hydrocephalic animals against cerebrospinal fluid (CSF) stroke volume in the cerebral aqueduct. There was no correlation in either group. For comparison, PI is plotted for all control animals, with stroke volumes taken from the mean control stroke volume of a previous study (Wagshul *et al*, 2009). The plot clearly indicates that even in cases where the ventricular CSF pulsatility is markedly elevated (with a 10- to 500-fold increase compared with normal) there is no increase in cortical microvascular pulsatility.

on these depth-by-group and heart rate-by-group associations, we conducted a *post hoc* test to identify subgroups of pulsatility measurements responsible for these differences. This analysis revealed that the subgroups with the deepest vessels were primarily responsible for the significant differences between the groups, with a significantly higher pulsatility in controls compared with hydrocephalic animals.

While more detailed investigations will clearly be needed to fully explain these results, we can offer a few plausible explanations. The most likely candidate to explain changes in pulsations in the brain is intracranial compliance, based on the well-known pressure–volume relationship (Marmarou *et al*, 1975). Marmarou showed that the exponential pressure–volume relationship in the brain leads to larger pressure pulsatility with either an increase in intracranial pressure or a decrease in intracranial compliance. Given that the primary sources of intracranial compliance are the veins and CSF-filled subarachnoid spaces (because of their direct communication with the compliant thecal sac), an increase in PI with depth may simply be a result of the increased distance from these sources of compliance. Furthermore, based on these assumptions our results of an overall decrease in pulsatility with hydrocephalus would be a reflection of increased brain compliance, which while counterintuitive is in agreement with recent direct measurements of locally increased compliance in hydrocephalus using magnetic resonance elastography (Streitberger *et al*, 2011). It should be noted, however, that these results are in sharp contrast with findings from several other studies showing decreased compliance in hydrocephalus (Bateman, 2000; Gonzalez-Darder and Barcia-Salorio, 1989; Marmarou *et al*, 1975; Miyati *et al*, 2003). It may be that our localized capillary measurements as well as magnetic resonance elastography are effectively measures of local tissue compliance, which increases in hydrocephalus while the classic CSF infusion studies probe the global compliance of the entire craniospinal system, which decreases in hydrocephalus.

Limitations

One potential limitation of the study is related to the anesthesia delivery. Since an injectable anesthetic was used with supplemental boluses as needed rather than a continuous infusion, the level of anesthesia varied over time, and may have been responsible for some of the variability in pulsatility. In particular, studies of the effect of hypercapnia on pressure pulsatility show that the systemic arterial and CSF pulse amplitudes are elevated with hypercapnia, with the latter attributed to capillary dilation (Avezaat *et al*, 1980; Portnoy and Chopp, 1981). However, there is a clear correlation between anesthesia depth (and thus potentially hypercapnia, due to depressed respiratory rate) and HR. If anything, our data show increased pulsatility in controls with increased HR, not the reverse, and no change in hydrocephalic animals. A further possible concern is the effect of anesthesia on cerebral blood flow. Ketamine–xylazine has been shown to cause a decrease in cerebral flow as compared with isoflurane (Lei *et al*, 2001; Masamoto *et al*, 2010). However, this is an effect on mean blood flow and the effects of ketamine–xylazine on flow pulsatility are not known. Moreover, because all animals received the same anesthetic regimen, we do not expect the particulars of the anesthesia to have affected our final conclusions.

Making an opening in the skull may irreversibly alter intracranial dynamics, by increasing intracranial compliance, minimizing any changes in pulsatility that may have existed. However, the cranial window was immediately sealed, and was carefully observed under the surgical microscope to ensure that no air bubbles had been left within the craniectomy and that the seal was complete. In addition, experiments were performed in both acute and chronic hydrocephalus animals, which presumably have different levels of elevated intracranial pressure (anecdotally, there was slightly more brain herniation through the craniectomy in acute animals) and no difference was found between these groups. Nonetheless, our null results were consistent in both groups of animals, implying that changes in intracranial dynamics from making the cranial window did not affect the results.

Ventriculomegaly was less pronounced in the chronic CH group compared with the acute CH group. The VVs of these animals clearly fit our criteria for hydrocephalus, with enlarged ventricles as well as elevated CSF SV compared with controls. Ventricular dilation in this hydrocephalus model, as in many other hydrocephalus models, generally varies over a wide range, and we have to consider it an unfortunate, unexplained coincidence that all

animals in the chronic CH group were only mildly hydrocephalic. We have shown in a prior study, as well as our extensive unpublished experience with this model, that chronic animals can experience the entire range of mild-to-severe ventricular dilation (Wagshul *et al*, 2009). Nonetheless, even with the limited ventriculomegaly in this group, we were able to show that hydrocephalus leads to reduced capillary pulsatility compared with controls at the deeper cortical levels.

Differentiating Flow and Pressure Pulsatility

To understand the implications of our results, and how they might relate to other measurements of pulsatility in the literature, a brief explanation is in order regarding the important difference between cardiac-induced pulsations in pressure waves as opposed to pulsations in flow velocity within CSF or vascular spaces; for a complete overview, the reader is referred to a recent review article on the topic (Wagshul *et al*, 2011). Briefly, all cardiac-induced pulsations in the brain can be assumed to originate from variations in pressure and flow in the carotid and basilar arteries feeding into the brain. In hydrocephalus, studies have shown changes in both intracranial pressure pulsatility (Carrera *et al*, 2010; Eide *et al*, 2007; Eide and Sorteberg, 2008; Eide and Saehle, 2010; Hu *et al*, 2008) and flow pulsatility (Bakker *et al*, 2002; Baledent *et al*, 2001; Bateman *et al*, 2005; Kahlon *et al*, 2007; Leliefeld *et al*, 2009; Miyati *et al*, 2003; Nadvi *et al*, 1995). However, a critical distinction between pressure and flow effects is that pressure waves are transmitted very rapidly throughout the brain, so that pressure pulsations within the ventricle, for example, are nearly identical to those measured within the parenchyma. Flow, however, relies on the physical transfer of fluid from one compartment to another, and therefore marked differences in flow velocities, and in flow pulsatility, can exist from one part of the brain to another. Therefore, one cannot necessarily reach any conclusions with respect to flow pulsatility based on the pressure pulsatility literature or vice versa. For example, even in the presence of elevated pressure pulsations throughout the brain, flow pulsations may be normal in certain compartments, since flow pulsations depend on the existence of a pressure pulsation gradient across the flow compartment (e.g., from the arterial to the venous side of a capillary bed). Thus, the discussions below are restricted to observations of flow pulsations in hydrocephalus alone.

Significance of Pulsatility in Communicating Hydrocephalus

The primary motivation for studying capillary pulsatility in hydrocephalus was to elucidate a possible role of microvascular pulsations in the pathogenesis of hydrocephalus. While ventriculomegaly is a well-explained phenomenon in cases with a clear obstruction to ventricular outflow, in CH clear-cut explanations for the mechanisms of ventricular dilation are lacking (Egnor *et al*, 2002; Greitz, 2004). A number of early studies suggested that ventricular dilation in CH may be a result of elevated ventricular pulsations, and that reduction of the CSF pulse wave can inhibit ventricular dilation (Bering, 1962; Wilson and Bertan, 1967). The most striking evidence came from a study showing that ventricular dilation could be induced in the absence of any CSF obstruction by artificially elevating the CSF pulse wave with a pulsating, intraventricular balloon (Pettorossi *et al*, 1978). Finally, elevated pulsations have also been extensively reported in clinical studies (Bradley *et al*, 1996; Greitz *et al*, 1994; Luetmer *et al*, 2002; Miyati *et al*, 2003). While there have been some attempts to use measures of CSF pulsatility to guide shunt surgery (Bradley *et al*, 1996), a number of recent trials have shown this to be an inadequate indicator of shunt success (Algin *et al*, 2010; Dixon *et al*, 2002; Kahlon *et al*, 2007).

To understand the connection between ventricular CSF pulsations and pulsatility at the capillary level, it is important to realize that almost all pulsatility in the brain is cardiac in nature and originates from the arterial vasculature. However, the route of pulsations from the arteries into the ventricles is still debated (Bering, 1962; Du Boulay, 1966; Egnor *et al*, 2002; Greitz, 2004). Since no studies have shown increased *arterial* pulsations in CH (in fact, studies have shown decreased intracranial arterial pulsations; Bateman and Loiselle, 2007), increased ventricular CSF pulsations in CH most likely arise from changes in the transfer and dissipation of arterial-driven pulsations within the cranium. One hypothesis is that CH is caused by a global redistribution of arterial pulsations, and a key prediction of this theory is increased capillary pulsatility (Greitz, 2004).

This pulsatility redistribution theory posits that arterial pulsations entering the brain are normally dampened via the Windkessel mechanism (Fung, 1997) and coupled into subarachnoid CSF, extracerebral veins, and venous sinuses. This gives rise to extracerebral venous pulsatility and pulsatile CSF flow in the SAS, which has been measured by magnetic resonance imaging at the foramen magnum (Alperin *et al*, 2000; Quigley *et al*, 2004). In CH, decreased global intracranial compliance may disrupt the normal intracranial flow dynamics, diminishing the transfer of arterial pulsations into subarachnoid CSF and veins and producing a decrease in CSF pulsatility at the foramen magnum (Greitz, 1993). In particular, in our model of basal cistern obstruction mimicking clinical cases such as subarachnoid hemorrhage and meningitis that also block this pathway, one would expect a decrease in pulsations transferred through the basal cisterns into the spinal SAS. With the removal of this major pulsatility dissipation pathway, arterial pulsations can propagate

undampened into the intracranial microvasculature, which has recently been shown to affect normal hemodynamics (Silacci *et al*, 2001; Ziegler *et al*, 1998). Furthermore, increased pulsatility of the entire intracranial microvasculature would be expected to result in increased brain pulsatility, which acting on the walls of the lateral ventricles would produce the well-documented increased ventricular CSF pulsatility. So, this theory predicts that undampened arterial pulsations will be transmitted into the microvasculature, and should be detectable as increased flow pulsation in cerebral capillaries.

The present study was thus designed to detect increased flow pulsations in neocortical capillaries with the induction of CH as a test of a pulsatility redistribution theory. We have shown that, at least on initial analysis, this theory is not correct: neocortical capillaries do not exhibit increased pulsatility with hydrocephalus induction. On the contrary, we have shown a significant decrease in capillary pulsatility with hydrocephalus, and have argued that these changes may be a product of the compliance changes in the hydrocephalic brain.

Alternate Explanations for Low Pulsatility

Based on our findings, we would conclude that (1) the redistribution theory is not an accurate representation of intracranial flow dynamics in hydrocephalus, or (2) pulsatility redistribution only causes local changes in pulsatility, such as in the choroid plexus or periventricular tissue, or (3) there is no relationship between macroscopic CSF flow pulsations and microscopic vascular pulsation. If increased capillary pulsatility is only manifest deep within the periventricular regions, and is not apparent in the superficial neocortical layers, our technique would not be capable of showing such changes. Our maximum imaging depth was 0.5 mm, while the depth of the periventricular white matter is $\sim$1.5 mm in our most severely hydrocephalic rats. The theoretical maximum imaging depth for multiphoton microscopy is $\sim$1 mm without resorting to much more invasive surgical procedures; recent advances have allowed *in vivo* multiphoton imaging in the mouse down to 1 mm (Kobat *et al*, 2009). Optical coherence tomography allows deeper imaging but does not provide the resolution required for capillary imaging. A second possibility is that capillary pulsatility is elevated only transiently, immediately after induction of CH during the period when the ventricles are initially undergoing dilation. We know from our previous studies that the majority of ventricular dilation occurs within a few days after induction of CH (Wagshul *et al*, 2009). By the time ventricular dilation has stabilized, the enlarged ventricles may be masking or compensating for elevated capillary pulsations, giving rise to diminished capillary pulsatility. Such a hypothesis will be addressed in future studies.

Conclusion

This study is the first attempt to measure capillary pulsatility deep in the rat neocortex. We have shown that capillary pulsatility normally increases with increasing depth from the pial surface. Our attempt to provide supportive evidence for a pulsatility redistribution theory of CH showed that if such redistribution does occur either it is not evident as a global increase in flow pulsatility throughout the cranium or it is not evident in the later stages of hydrocephalus when ventricular size has stabilized. Furthermore, we found that the normal increase in pulsatility with depth disappears with hydrocephalus induction, and explanations of this effect based on local intracranial compliance changes have been suggested. Future studies will investigate capillary pulsatility at earlier time points, potentially within hours of induction, when the kaolin blockage may cause changes in pulsation distributions but ventricular enlargement has not yet occurred.

Acknowledgements

The authors thank Dr Jie Li of SUNY Upstate Medical University for assistance with the surgical procedures, Dr Joseph Madsen of Harvard Medical School for help with the initial design of the experiments, and Dr Noam Alperin of the University of Miami for valuable discussions regarding the manuscript and interpretation of our results. The authors thank the Brain Child Foundation and STARS-kids Foundation for financial support of our work.

Disclosure/conflict of interest

The authors declare no conflict of interest.

References

Algin O, Hakyemez B, Parlak M (2010) The efficiency of PC-MRI in diagnosis of normal pressure hydrocephalus and prediction of shunt response. *Acad Radiol* 17:181–7

Alperin N, Sivaramakrishnan A, Lichtor T (2005) Magnetic resonance imaging-based measurements of cerebrospinal fluid and blood flow as indicators of intracranial compliance in patients with Chiari malformation. *J Neurosurg* 103:46–52

Alperin NJ, Lee SH, Loth F, Raksin PB, Lichtor T (2000) MR-Intracranial pressure (ICP): a method to measure intracranial elastance and pressure noninvasively by means of MR imaging: baboon and human study. *Radiology* 217:877–85

Avezaat CJ, van Eijndhoven JH, Wyper DJ (1980) Effects of hypercapnia and arterial hypotension and hypertension on cerebrospinal fluid pulse pressure and intracranial volume-pressure relationships. *J Neurol Neurosurg Psychiatry* 43:222–34

Bakker SL, Boon AJ, Wijnhoud AD, Dippel DW, Delwel EJ, Koudstaal PJ (2002) Cerebral hemodynamics before and

after shunting in normal pressure hydrocephalus. *Acta Neurol Scand* 106:123–7

Baledent O, Henry-Feugeas MC, Idy-Peretti I (2001) Cerebrospinal fluid dynamics and relation with blood flow: a magnetic resonance study with semiautomated cerebrospinal fluid segmentation. *Invest Radiol* 36: 368–77

Bateman GA (2000) Vascular compliance in normal pressure hydrocephalus. *AJNR Am J Neuroradiol* 21: 1574–85

Bateman GA, Levi CR, Schofield P, Wang Y, Lovett EC (2005) The pathophysiology of the aqueduct stroke volume in normal pressure hydrocephalus: can co-morbidity with other forms of dementia be excluded? *Neuroradiology* 47:741–8

Bateman GA, Loiselle AM (2007) Can MR measurement of intracranial hydrodynamics and compliance differentiate which patient with idiopathic normal pressure hydrocephalus will improve following shunt insertion? *Acta Neurochir (Wien)* 149:455–62; discussion 62

Bering Jr EA (1962) Circulation of the cerebrospinal fluid. Demonstration of the choroid plexuses as the generator of the force for flow of fluid and ventricular enlargement. *J Neurosurg* 19:405–13

Bilfinger TV, Stefano GB (2000) Human aortocoronary grafts and nitric oxide release: relationship to pulsatile pressure. *Ann Thorac Surg* 69:480–5

Bradley WG, Jr, Scalzo D, Queralt J, Nitz WN, Atkinson DJ, Wong P (1996) Normal-pressure hydrocephalus: evaluation with cerebrospinal fluid flow measurements at MR imaging. *Radiology* 198:523–9

Carrera E, Kim DJ, Castellani G, Zweifel C, Czosnyka Z, Kasprowicz M, Smielewski P, Pickard JD, Czosnyka M (2010) What shapes pulse amplitude of intracranial pressure? *J Neurotrauma* 27:317–24

Denk W, Strickler JH, Webb WW (1990) Two-photon laser scanning fluorescence microscopy. *Science* 248: 73–6

Dixon GR, Friedman JA, Luetmer PH, Quast LM, McClelland RL, Petersen RC, Maher CO, Ebersold MJ (2002) Use of cerebrospinal fluid flow rates measured by phase-contrast MR to predict outcome of ventriculoperitoneal shunting for idiopathic normal-pressure hydrocephalus. *Mayo Clin Proc* 77:509–14

Du Boulay GH (1966) Pulsatile movements in the CSF pathways. *Br J Radiol* 39:255–62

Egnor M, Zheng L, Rosiello A, Gutman F, Davis R (2002) A model of pulsations in communicating hydrocephalus. *Pediatr Neurosurg* 36:281–303

Eide PK, Egge A, Due-Tonnessen BJ, Helseth E (2007) Is intracranial pressure waveform analysis useful in the management of pediatric neurosurgical patients? *Pediatr Neurosurg* 43:472–81

Eide PK, Saehle T (2010) Is ventriculomegaly in idiopathic normal pressure hydrocephalus associated with a transmantle gradient in pulsatile intracranial pressure? *Acta Neurochir (Wien)* 152:989–95

Eide PK, Sorteberg W (2008) Changes in intracranial pulse pressure amplitudes after shunt implantation and adjustment of shunt valve opening pressure in normal pressure hydrocephalus. *Acta Neurochir (Wien)* 150: 1141–7; discussion 7

Fung YC (1997) *Biomechanics: Circulation*. 2nd ed. New York: Springer

Gonzalez-Darder JM, Barcia-Salorio JL (1989) Pulse amplitude and volume-pressure relationships in experimental hydrocephalus. *Acta Neurochir (Wien)* 97:166–70

Gosling RG, King DH (1974) Arterial assessment by Doppler-shift ultrasound. *Proc R Soc Med* 67:447–9

Greitz D (1993) Cerebrospinal fluid circulation and associated intracranial dynamics. A radiologic investigation using MR imaging and radionuclide cisternography. *Acta Radiol Suppl* 386:1–23

Greitz D (2004) Radiological assessment of hydrocephalus: new theories and implications for therapy. *Neurosurg Rev* 27:145–65; discussion 66–7

Greitz D, Hannerz J, Rahn T, Bolander H, Ericsson A (1994) MR imaging of cerebrospinal fluid dynamics in health and disease. On the vascular pathogenesis of communicating hydrocephalus and benign intracranial hypertension. *Acta Radiol* 35:204–11

Hu X, Xu P, Lee DJ, Paul V, Bergsneider M (2008) Morphological changes of intracranial pressure pulses are correlated with acute dilatation of ventricles. *Acta Neurochir Suppl* 102:131–6

Jones HC, Bucknall RM, Harris NG (1991) The cerebral cortex in congenital hydrocephalus in the H-Tx rat: a quantitative light microscopy study. *Acta Neuropathol* 82:217–24

Kahlon B, Annertz M, Stahlberg F, Rehncrona S (2007) Is aqueductal stroke volume, measured with cine phase-contrast magnetic resonance imaging scans useful in predicting outcome of shunt surgery in suspected normal pressure hydrocephalus? *Neurosurgery* 60: 124–9; discussion 9–30

Kleinfeld D, Mitra PP, Helmchen F, Denk W (1998) Fluctuations and stimulus-induced changes in blood flow observed in individual capillaries in layers 2 through 4 of rat neocortex. *Proc Natl Acad Sci USA* 95: 15741–6

Kobat D, Durst ME, Nishimura N, Wong AW, Schaffer CB, Xu C (2009) Deep tissue multiphoton microscopy using longer wavelength excitation. *Opt Express* 17: 13354–64

Lei H, Grinberg O, Nwaigwe CI, Hou HG, Williams H, Swartz HM, Dunn JF (2001) The effects of ketamine-xylazine anesthesia on cerebral blood flow and oxygenation observed using nuclear magnetic resonance perfusion imaging and electron paramagnetic resonance oximetry. *Brain Res* 913:174–9

Leliefeld PH, Gooskens RH, Peters RJ, Tulleken CA, Kappelle LJ, Han KS, Regli L, Hanlo PW (2009) New transcranial Doppler index in infants with hydrocephalus: transsystolic time in clinical practice. *Ultrasound Med Biol* 35:1601–6

Li J, McAllister JP, II, Shen Y, Wagshul ME, Miller JM, Egnor MR, Johnston MG, Haacke EM, Walker ML (2008) Communicating hydrocephalus in adult rats with kaolin obstruction of the basal cisterns or the cortical subarachnoid space. *Exp Neurol* 211:351–61

Luciano MG, Skarupa DJ, Booth AM, Wood AS, Brant CL, Gdowski MJ (2001) Cerebrovascular adaptation in chronic hydrocephalus. *J Cereb Blood Flow Metab* 21: 285–94

Luetmer PH, Huston J, Friedman JA, Dixon GR, Petersen RC, Jack CR, McClelland RL, Ebersold MJ (2002) Measurement of cerebrospinal fluid flow at the cerebral aqueduct by use of phase-contrast magnetic resonance imaging: technique validation and utility in diagnosing idiopathic normal pressure hydrocephalus. *Neurosurgery* 50:534–43; discussion 43–4

Marmarou A, Shulman K, LaMorgese J (1975) Compartmental analysis of compliance and outflow resistance of the cerebrospinal fluid system. *J Neurosurg* 43:523–34

Masamoto K, Obata T, Kanno I (2010) Intracortical microcirculatory change induced by anesthesia in rat somatosensory cortex. *Adv Exp Med Biol* 662:57–61

Mauer UM, Freude G, Danz B, Kunz U (2008) Cardiac-gated phase-contrast magnetic resonance imaging of cerebrospinal fluid flow in the diagnosis of idiopathic syringomyelia. *Neurosurgery* 63:1139–44; discussion 44

Miyati T, Mase M, Banno T, Kasuga T, Yamada K, Fujita H, Koshida K, Sanada S, Onoguchi M (2003) Frequency analyses of CSF flow on cine MRI in normal pressure hydrocephalus. *Eur Radiol* 13:1019–24

Nadvi SS, Van Dellen JR, Gouws E (1995) Transcranial Doppler ultrasonography in hydrocephalic children with tuberculous meningitis. *Br J Neurosurg* 9:519–26

Pettorossi VE, Di Rocco C, Mancinelli R, Caldarelli M, Velardi F (1978) Communicating hydrocephalus induced by mechanically increased amplitude of the intraventricular cerebrospinal fluid pulse pressure: rationale and method. *Exp Neurol* 59:30–9

Portnoy HD, Chopp M (1981) Cerebrospinal fluid pulse wave form analysis during hypercapnia and hypoxia. *Neurosurgery* 9:14–27

Quigley MF, Iskandar B, Quigley ME, Nicosia M, Haughton V (2004) Cerebrospinal fluid flow in foramen magnum: temporal and spatial patterns at MR imaging in volunteers and in patients with Chiari I malformation. *Radiology* 232:229–36

Silacci P, Desgeorges A, Mazzolai L, Chambaz C, Hayoz D (2001) Flow pulsatility is a critical determinant of oxidative stress in endothelial cells. *Hypertension* 38:1162–6

Streitberger KJ, Wiener E, Hoffmann J, Freimann FB, Klatt D, Braun J, Lin K, McLaughlin J, Sprung C, Klingebiel R, Sack I (2011) *In vivo* viscoelastic properties of the brain in normal pressure hydrocephalus. *NMR Biomed* 24:385–92

Wagshul ME, Eide PK, Madsen JR (2011) The pulsating brain: a review of experimental and clinical studies of intracranial pulsatility. *Fluids Barriers CNS* 8:5

Wagshul ME, McAllister JP, Rashid S, Li J, Egnor MR, Walker ML, Yu M, Smith SD, Zhang G, Chen JJ, Benveniste H (2009) Ventricular dilation and elevated aqueductal pulsations in a new experimental model of communicating hydrocephalus. *Exp Neurol* 218:33–40

Wilson CB, Bertan V (1967) Interruption of the anterior choroidal artery in experimental hydrocephalus. *Arch Neurol* 17:614–9

Ziegler T, Bouzourene K, Harrison VJ, Brunner HR, Hayoz D (1998) Influence of oscillatory and unidirectional flow environments on the expression of endothelin and nitric oxide synthase in cultured endothelial cells. *Arterioscler Thromb Vasc Biol* 18:686–92